Polarization-modulating switchable and selectable image display through an ultrathin quasi-bound-state-in-the-continuum metasurface

Zonglin Li,[1,2] Guozheng Nie,[1,2,*] Junhui Wang,[1,2] Fang Zhong,[1,2] and Shiping Zhan[1,2]

[1] *School of Physics and Electronic Science, Hunan University of Science and Technology, Xiangtan, Hunan 411201, China*

[2] *Hunan Provincial Key Laboratory of Intelligent Sensors and New Sensor Materials, Xiangtan, Hunan 411201, China*

(Received 27 September 2023; revised 4 November 2023; accepted 1 March 2024; published 20 March 2024)

Active manipulation on absorption takes an essential place in nanophotonic light modulators, which always suffer from static tuning ability, limited depth, and insufficient modulating efficiency. In this study, we propose an alternative strategy utilizing the symmetry-protected-type bound state in the continuum (SPBIC) to satisfy a tunable critical-coupling absorber with high modulating mobility. To demonstrate our concept, we illustrate an ultrathin critical-coupling absorbing system composed of germanium metasurface and monolayer graphene through elaborately maneuvered quasi-SPBIC, which provides substantial local field enhancement to boost the light absorption of graphene. The intensity of such critical-coupling absorption can be efficiently tuned by modulating the polarization of the incident waves with an efficiency of 97.1%. Via this polarization control, we demonstrate digital switch "0-1" and switchable and selectable image-displaying functions in simulation. Such functions are obtained in one single-designed array by incident polarization while requiring no additional structural change. Our results may pave the way for next-gen nanophotonic metadevices.

DOI: 10.1103/PhysRevApplied.21.034039

I. INTRODUCTION

Nowadays, modern nanophotonics aims to efficiently manipulate optical properties at the nanoscale for integrating multiple optical functions in a single compact chip, which makes sense in ultrafast switching and information processing in optics [1,2]. Generated by coupling between the photons in the incident wave and the electrons in metals or insulators, surface plasmon polaritons (SPPs) can exceed the diffraction limit of traditional optics to localize light in the subwavelength range. As a result, metasurfaces based on the SPP mechanism, especially the SPP perfect absorbers, have been widely applied in sensing, communicating, and imaging [3–6]. Nevertheless, there are many natural flaws in SPP absorbers based on precious metals. For example, the majority of SPP absorbers have high Ohmic loss and allow only static regulation, which hinders the applications in practice.

High-index dielectric metasurfaces, expected to be promising alternatives to plasmonic metasurfaces, have emerged in widespread applications [7,8]. Utilizing the control over the induced electromagnetic Mie resonances, all-dielectric metasurfaces can offer efficient light localization and manipulation, providing excellent application potentials in future on-chip device designs [8–10]. In recent years, many different kinds of all-dielectric metasurfaces that support Fano and magnetic dipole (MD) resonances have been studied to restrain and maneuver light in a subwavelength scale [11–13]. On the other hand, due to the nature of flexible tunability, low Ohmic loss, strong locality, and ultracompact configuration, graphene, the most famous two-dimensional (2D) material, has attracted tremendous interest from researchers. Regrettably, being the obstacle to application, monolayer graphene has a frail light absorption of 2.3% in the visible and infrared ranges [14], resulting in weak light-matter interaction.

Bound states in the continuum (BICs), initially mentioned as a theory in quantum mechanics [15], have been broadly researched in multiple fields of wave physics: water [16], acoustics [17,18], microwaves [19], and nanophotonic optics [20–22]. In specially designed periodic nanophotonic structures under the free-space light cone, some exceptional cases of Fano resonances generated from the coupling between two resonances, which have different damping rates, can collapse to a BIC with the theoretically infinite quality (Q) factor, leading the Fano features to vanish as the resonance becomes ideally unable to couple with free-space radiations [19,23]. Notably, in a symmetrical periodic structure, such as in a photonic crystal slab, the modes above the light cone in the band structure can couple to the continuum of the extended modes. Therefore, they are generally radiative.

*gzhnie@hnust.edu.cn

Nevertheless, on account of the symmetry mismatch between the mode profiles and the external propagating modes, some bound states can even exist at Γ point above the light cone. When the operating frequency at Γ point is lower than the diffraction limit, the only radiating state will be the plane wave in the normal direction with an odd electromagnetic field under C_2 symmetry [24,25]. In this circumstance, all even modes at Γ point are BICs, the mode profiles of which show no overlap with radiating waves, and such a unique BIC is called the symmetry-protected (SP)BIC. Practically, by introducing microstructural perturbation to disrupt the symmetry so that an SPBIC can couple with the extended states in the continuum, it can be transformed into the quasi-bound-states in the continuum (QBICs), which is a type of leaky mode with tremendous but finite Q factors, appearing close to the BIC [26]. The extraordinary Q factor of a QBIC can impulse massive enhancement on the local electric field in the nanoscale [27], which can heighten the light-matter interactions and is believed to support promising applications in sensors [28], lasers [29], absorbers [30], and nonlinear devices [31,32]. As an alternative method to promote light-matter interaction, the QBIC mechanism is rarely mentioned in graphene-based absorbers.

In this work, another strategy to achieve critical-coupling absorption by utilizing the SPBIC is proposed, and the potential alternative applications in optical switching and image displaying are discussed. First, an all-dielectric metasurface is demonstrated, which supports an SPBIC in the long-wave-infrared (LWIR) range. By introducing perturbation to disrupt the in-plane symmetry, such an SPBIC can be transformed into QBICs and significantly enhances the local electric field. Then we introduce the monolayer graphene (MG) into the resonator system, and the light absorption of it is enormously boosted by the QBIC resonance in the metasurface, and by tuning the Fermi level E_F of MG and optimizing the asymmetry parameter of the metasurface, critical-coupling absorption is satisfied. Behaviors of the absorption band are analyzed, and the results indicate high mobility on active tuning for both wavelength and bandwidth. Further studies show that the intensity of such critical-coupling absorption can be efficiently tuned by the polarization angle of the incident wave, leading to a high modulating efficiency reaching 97.1%, which exceeds several existing works [33–35]. Performance of designs for optical "0-1" digital switch and switchable and selectable image display is demonstrated based on such polarization-sensitive features, indicating promising potential for next-gen nanophotonics applications.

II. SIMULATIONS AND RESULT ANALYSES

The geometrical diagrams of one single unit cell for our proposed all-dielectric metasurface with in-plane broken symmetry are illustrated in Fig. 1. The period of the unit cell is $p_x = p_y = 1000$ nm. The outer and inner radii of the Ge nanoring on the SiO_2 substrate are $r_o = 370$ nm and $r_i = 120$ nm. As is shown in Fig. 1(b), the split with an angle θ, symmetrical along the x-z plane, which crosses the x axis, is introduced to break the in-plane symmetry, making it a C-shaped ring. In Fig. 1(c), the $z = 0$ nm plane is defined as the interface of the Ge ring and the substrate. The ring's thickness $h_1 = 100$ nm. Commercial software Lumerical FDTD Solutions is used to conduct our simulations and analyses. Ge (Germanium)-Palik model in the material database of FDTD Solutions is used to fit the index of Ge, and the index of SiO_2 is set as 1.44 for the convenience of simulation. For the simulating region, periodic boundary conditions are set in x and y directions, while the perfect-match layers (PMLs) are set in z directions. A uniform mesh with the step sizes d$x = 7$ nm, d$y = 7$ nm, and d$z = 10$ nm is set. Auto shutoff min remains the default 1×10^{-5}, and the structure system is excited by a plane wave propagating along $-z$ direction and polarizing along y directions with amplitude $|E| = 1$, unless otherwise noted.

As illustrated in Fig. 2(a), we first consider an ideally standalone array (without the SiO_2 substrate) composed of the original symmetrical hollow Ge nanorings without the split θ. Bloch boundary conditions in x and y directions and a dipole cloud are utilized to excite all the modes supported by the array. Figure 2(b) shows the photonic band structure of this array, revealing that this periodic ring array supports an SPBIC eigenmode at the Γ point in the first Brillouin zone. Such a BIC originates from the magnetic dipole (MD) resonance supported by the exquisitely designed nanorings at the Γ point, with its corresponding frequency

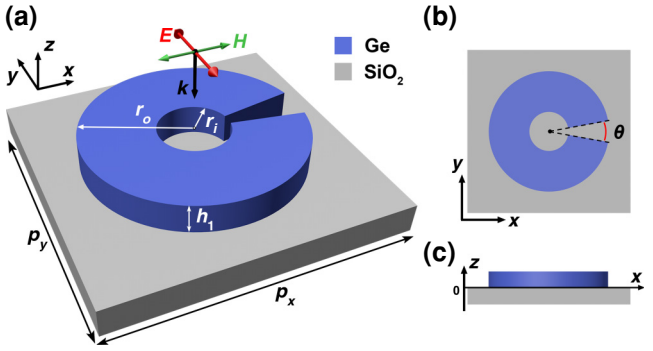

FIG. 1. (a) Schematic of the proposed all-dielectric metasurface. The parameters: $p_x = p_y = 1000$ nm, $r_i = 120$ nm, $r_o = 370$ nm, and $h_1 = 100$ nm. The thickness of the SiO_2 substrate is infinite. (b) Schematic of breaking the in-plane symmetry. A split with an angle θ, which is symmetrical along the x-z plane crossing the x axis, is set on a side of the Ge ring. The asymmetry parameter s is accordingly defined as $\rho = \sin\theta/2$. (c) Schematic of the front view of the metasurface. The interface between the Ge ring and the SiO_2 substrate is defined as the $z = 0$ nm plane.

below the diffraction limit of the given periodic structure. Under this circumstance, the only radiating states are the plane waves spreading in normal directions, with the electromagnetic field vectors being odd under C_2 symmetry [22,36]. Therefore, due to the symmetry mismatch, the MD mode becomes entirely "trapped" and unable to couple with modes in the free space, leading to the theoretical infinite Q factor. As shown in Fig. 2(c), the excited-field energy is strongly confined in the Ge ring, with the typical in-plane circulating displacement currents, which is the character of an MD mode. Figure 2(d) demonstrates the far-field electric distribution of such an eigenmode, also showing the typical MD radiation pattern of Mie-like modes. When the perturbation is introduced to break the in-plane symmetry, such an unstable SPBIC can be transformed into QBICs.

We have proved the statement above through our simulations. For examining the resonance situations in the proposed metasurface, the Ge ring with the proposed symmetry-breaking split is placed on a SiO_2 substrate. (It is worth noticing that, in the practical preparation, generally, the substrate is of huge contrast in thickness compared with the metasurface, so we set the thickness of the substrate infinite in our simulations for simplification.) and transmission spectra under variant split angle θ are analyzed. As is shown in Fig. 3(a), when in-plane symmetry is disrupted by the introduced split as the perturbation, narrow dips appear in the transmission spectra, which nicely fits the classic Fano resonance line shape [17], represented in the following formula:

$$\mathbf{T}(\omega) = \mathbf{T}_0 + a_0 \frac{(q + 2(\omega - \omega_0)/\zeta)^2}{1 + (2(\omega - \omega_0)/\zeta)^2}, \tag{1}$$

where $\mathbf{T}_0$ is the background transmission, a_0 and q are constant real coefficients, ω_0 is the resonant frequency, and ζ is the overall resonant damping rate of the resonator. The electric distributions of the QBIC mode under $\theta = 8^\circ$ in Fig. 3(b) shows that the electric field inside the gap area is significantly enhanced. The result in Fig. 3(c), where we conduct the multipole expansion for the case of $\theta = 8^\circ$ through an open-source method provided by Hinamto and Fujii [37], can help to understand the mechanism behind. The expansion shows that such QBIC resonance is dominated by the MD response, while the contribution from the electric dipole (ED), which represents the radiating channel coupling to the outgoing waves, is small. When one breaks the in-plane symmetry, the MD's opposite dipole moments become no longer equal, which makes the system's net dipole moment nonzero. Therefore, the "trapped" MD mode at the Γ point is no longer confined, which means it becomes able to couple and exchange energy with other modes in the free space, leading to tremendous local-field enhancement in the split, and showing the asymmetric Fano shape. Additionally, the features of QBIC mode are

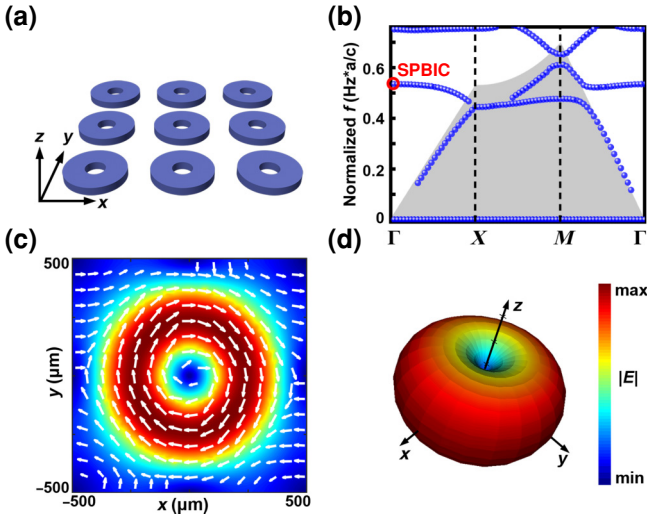

FIG. 2. (a) Schematic of the periodic Ge-ring array. (b) Photonic band structure of the periodic Ge ring array. The confined symmetry-protected BIC is marked with a red circle. (c) The near-field electric distribution of the BIC eigenmode ($\lambda = 1870.01$ nm) presented for the $z = 50$ nm plane. The white arrows indicate the directions of in-plane displacement currents. (d) The far-field electric radiation pattern of the eigenmode.

closely related to θ: as is illustrated in Fig. 3(a), when θ increases in an appropriate range, the transmission dips will manifest slight blueshift and widening. In order to study these behaviors, Q factors of the QBIC modes under different θ are calculated in Fig. 3(d). Here, the asymmetry parameter s is defined as $s = \sin(\theta/2)$, and the Q factor is plotted as a function of s (under $\log_{10}$-$\log_{10}$ scale for intuitive illustration of the relationship between s and Q). The result shows that the Q factor acts an apparent behavior for s in a proper range, conforming with the inverse quadratic relationship:

$$Q(\theta) = Q_0 \left[s(\theta)\right]^{-2}. \tag{2}$$

Here, $s(\theta) = \sin(\theta/2)$ and Q_0 is a constant irrelevant to θ, which is determined by the structure [38]. The result indicates that one can actively tune the coupling rate effectively in the proposed metasurface. When monolayer graphene is introduced into this resonator system, its light absorption can be boosted by the strongly enhanced local field. Critical-coupling conditions for the absorber can be satisfied by utilizing such tunable features of the QBICs. And according to this mechanism, the absorber will also be actively tunable.

Such resonance features of QBIC we have found in such an all-dielectric metasurface are believed to be able to provide the enhancement on light-graphene interactions, which can be defined as a parameter by the light-absorbing

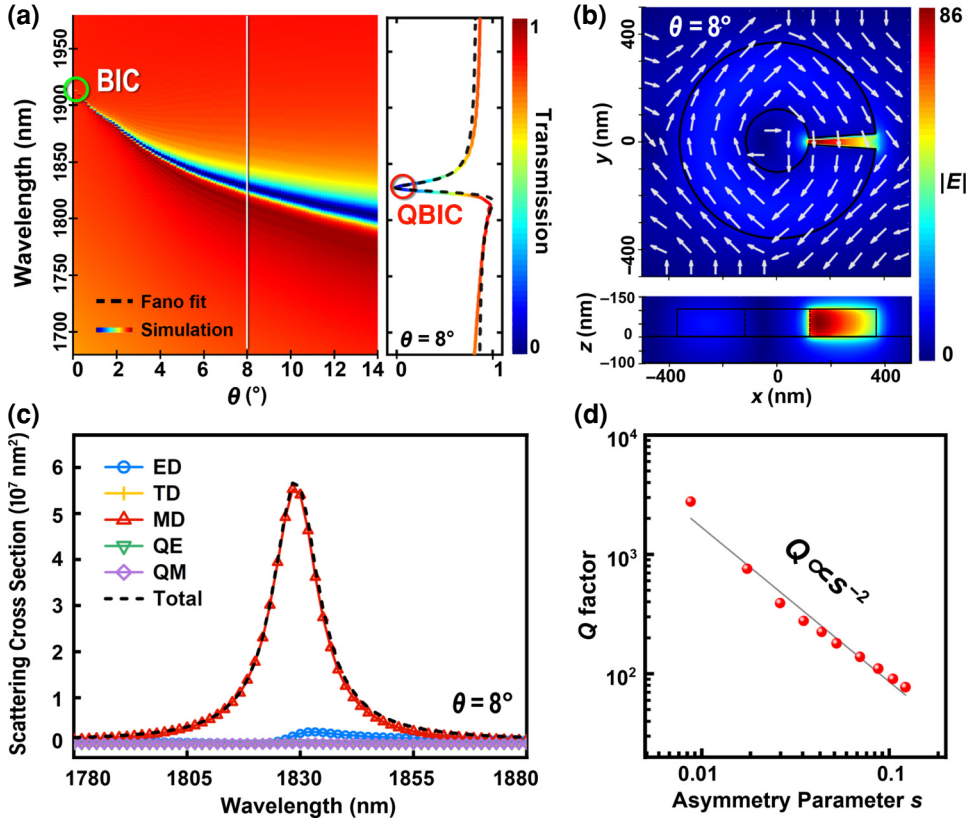

FIG. 3. (a) Transmission spectra of the metasurface with an infinite SiO_2 substrate when in-plane symmetry is broken with different split θ. The position of the example spectrum under $\theta = 8^\circ$ is indicated by a white line, and its simulated and Fano-fitted spectra is shown on the right side. (b) When $\theta = 8^\circ$, the electric energy field in the metasurface at the resonance point ($\lambda = 1826.09$ nm). The in-plane field vectors are indicated by white arrows. (c) The multipole expansion for the resonance under $\theta = 8^\circ$. (d) Graph of plotting Q factor as a function of the asymmetry parameter s (under $\log_{10}$–$\log_{10}$ scale).

efficiency [39]:

$$P_A(\omega) = 0.5\omega \int \varepsilon''(\omega)|E|^2(\omega)\mathrm{d}V. \tag{3}$$

Here, ω is a variant frequency, $\varepsilon''(\omega)$ is the imaginary dielectric constant, and $|E|$ is the electric field. The absorption power is integrated over the volume that graphene occupies. One can tell from this formula that, graphene's light-absorbing power is strongly correlated with the electric field overlapped between graphene and the dielectric metasurface. In our simulation, the monolayer graphene (MG) is modeled as a broad 2D dielectric layer covering the whole period, and placed on top of the C-shaped ring, which is the z = 100 nm plane, as illustrated in Fig. 4(a). The surface conductivity σ of MG is obtained through the Kubo model [40]:

$$\sigma(\omega, E_F, \Gamma, T) = N_g(\sigma_{intra} + \sigma_{inter}), \tag{4}$$

$$\sigma_{intra} = \frac{-ie^2}{\pi\hbar(\omega + 2i\Gamma)} \int_0^\infty \xi \left[\frac{\partial f_d(\xi)}{\partial \xi} + \frac{\partial f_d(-\xi)}{\partial \xi}\right] \mathrm{d}\xi, \tag{5}$$

$$\sigma_{inter} = \frac{ie^2(\omega + 2i\Gamma)}{\pi\hbar} \int_0^\infty \frac{\int_d(\xi) - f_d(\xi)}{(\omega + 2i\Gamma) - 4(\frac{\xi}{\hbar})^2} \mathrm{d}\xi, \tag{6}$$

where

$$f_d(\xi) = \left[\exp\left(\frac{\xi - E_F}{k_B T}\right) + 1\right]^{-1} \tag{7}$$

and

$$\Gamma = \frac{e v_F^2}{2\mu E_F} \tag{8}$$

is the scattering rate. The quantities in the model are as follows: $T = 300$ K is the temperature, $N_g = 1$ is the

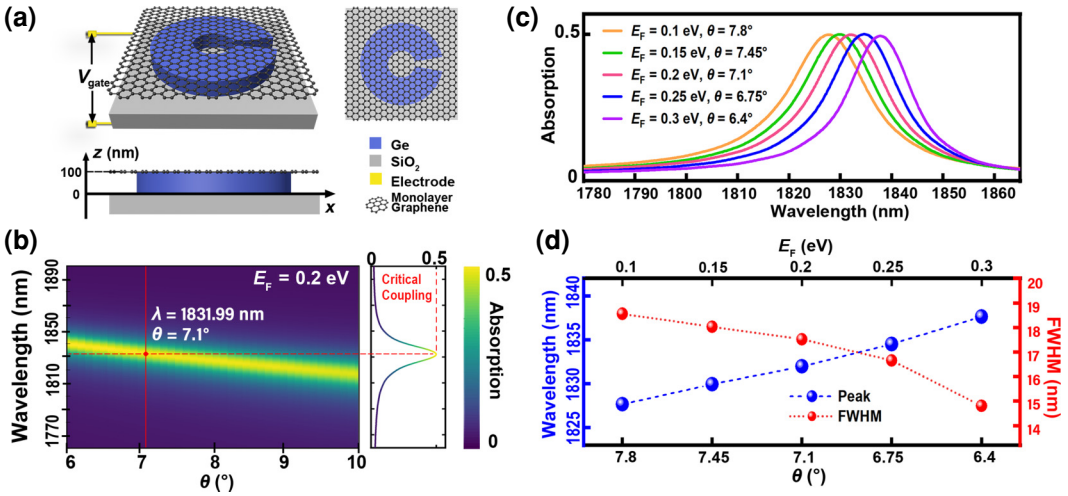

FIG. 4. (a) Schematics of the proposed graphene-metasurface system. Monolayer graphene (MG) is laid on top of the C ring, which is defined as the $z = 100$ nm plane. (b) Light-absorption spectra of the system under variant θs with MG $E_F = 0.2$ eV. The absorption under the critical-coupling condition when $\theta = 7.1^\circ$ is illustrated on the right. (c) Critical-coupling absorption spectra with different MGs $E_F = 0.1$, 0.15, 0.2, 0.25, and 0.3 eV. (d) For (c), the peak wavelength and FWHM of the absorption band as functions of θ and E_F.

number of the graphene layer, σ_{intra} is the intraband conductivity contribution, σ_{inter} is the interband conductivity contribution, $v_F = c/300 = 10^6$ m/s is the Fermi velocity, $\mu = 1\ m^2/(V\ s)$ is the carrier mobility, and E_F is the Fermi level of graphene. And it has been proved that in metasurfaces, one can actively tune E_F easily by applying gate voltage through electrodes placed on MG and the substrate [41], so for the purpose of simplification, we consider only MG on different E_F by varying the values of corresponding physical quantities in our simulations.

In this case, the light absorption of the graphene-metasurface system is calculated, and the results are shown in Fig. 4(b). Taking the monolayer graphene on the Fermi level $E_F = 0.2$ eV as an example, we sweep the light absorption with increasing θ, and get a blueshifting and widening boosted absorption band, which behaves correlatively with the transmission dip in Fig. 3(a) brought by the QBIC resonance. When analyzing the proposed graphene-metasurface as a single-mode optical resonator, according to the temporal coupled-mode theory (TCMT), the light absorption of the system can be presented as [42,43]

$$\mathbf{A} = \frac{2\gamma\delta}{(\omega-\omega_0)^2+(\delta+\gamma)^2}, \tag{9}$$

where γ is the radiation rate of the photonic resonator and δ is the dissipative loss rate of the absorbing material. In our proposed system, δ can be represented by the dissipative loss rate of MG, as it is the only lossy medium in the system. At the resonant frequency $\omega = \omega_0$, the maximum of absorption intensity is achieved, where the value $\mathbf{A}_0$ is determined only by the ratio of δ and γ as

$$\mathbf{A}_0 = \frac{2\gamma\delta}{(\delta+\gamma)^2} = \frac{2}{2+\frac{\gamma}{\delta}+\frac{\delta}{\gamma}}, \tag{10}$$

and once $\gamma = \delta$, the critical-coupling condition of this system will be satisfied, under which the two-port single-mode resonator will reach the theoretical maximized light absorption $\mathbf{A}_{max} = 0.5$. In other words, the complex eigenfrequency of a resonant leaky mode can be expressed as $\omega = \omega_0 - i\gamma$, and the radiative Q factor can be defined as $Q_R = \omega_0/2\gamma$. As for an absorptive medium, the Q factor of its intrinsic absorption $Q_A = \omega_0/2\delta$. Therefore the critical coupling condition can be described as $Q_R = Q_A$. Moreover, Q_A is also associated with the refractive index of the absorptive materials in a system [44]. For monolayer graphene, n_{MG} can be obtained from Refs. [45,46]. To obtain Q_A, the effective refractive index should be considered at first, which is a function of the index and thickness of MG and the Ge metasurface under normal incidence:

$$n_{eff} = \frac{n_{MG}t_{MG} + n_{Ge}h_1}{t_{MG}+h_1}, \tag{11}$$

where n_{MG} and n_{Ge} are the refractive index of monolayer graphene and germanium, respectively. $t_{MG} = 0.34$ nm is the thickness of MG. Take MG with $E_F = 0.2$ eV, for example, the effective refractive index is $n_{eff} = 4.11867 + 0.00988i$ at $\lambda = 1831.99$ nm, which makes $Q_A = \mathrm{Re}[n_{eff}]/2\mathrm{Im}[n_{eff}] = 208.4$. To match $Q_R = Q_A$, from the $Q - s$ relationship in Fig. 3(d) one can estimate that the target θ is around 7°. Finally when $\theta = 7.1^\circ$, the eigenfrequency of the QBIC is found to be $163.755 +$

$0.786i$ (THz), which makes $Q_R = 208.4$, satisfying the critical-coupling condition and bringing $\mathbf{A}_{max} = 0.5$ as shown in Fig. 4(b). For monolayer graphene, the surface conductivity δ changes with different E_F, which manipulates δ to vary [47,48]. In this study, we consider five kinds of monolayer graphene with increasing E_F from 0.1 to 0.3 eV. Calculation of the Kubo formula shows that δ decreases with the increasing E_F from 0.1 to 0.3 eV, which leads the dissipative loss rate δ of graphene to decay. To satisfy the critical-coupling condition $\gamma = \delta$, the radiation rate of the system γ should be tuned down, which means one, according to Fig. 3(c) should increase the split angle θ to tune down the coupling rate of the proposed metasurface.

The result in Fig. 4(c), which presents the critical-coupling absorption spectra under $E_F = 0.1$, 0.15, 0.2, 0.25, and 0.3 eV, has confirmed this claim above. When achieving critical-coupling conditions, θ decreases inversely with the increasing E_F. On the other hand, the features of the critical-coupling absorption band are analyzed in Fig. 4(d), where the wavelength point of the absorption peak and the FWHM, which is highly correlative with δ and γ as

$$\mathbf{W}_{max/2} = 2(\delta + \gamma) \tag{12}$$

are calculated as functions of E_F and θ. The result demonstrates that when θ increase under critical-coupling conditions, the absorption band also shows the behavior of linear blueshifting and widening, which is consistent with the result in Fig. 4(b). The above results indicate promising application in the field of tunable absorbers, for our proposed graphene-dielectric-metasurface hybrid resonator can not only satisfy single-mode critical-coupling absorption but also allow active adjustments on both the absorbing frequency position and bandwidth.

III. APPLICATION DISCUSSION

Generally speaking, the traditional applications of adjustable graphene-based absorbers concentrated on sensors or filters [49–51]. Here, we study the rarely mentioned applications: optical switch and image display, and introduce the possible potential applications based on our proposed graphene absorber. First, the polarization effect of the incident wave is considered. Because of MD's dependence on the incident polarization, the excitation of MD in the resonator will change as one rotates the incident polarization direction (noted as IPD). Such polarization-dependent performance originates from the interference of Mie-resonant multipoles [52,53]. Based on this, we introduce an alternative method to analyze the in-plane symmetry of the metasurface, which is to examine the symmetry relative to IPD. It is worthwhile to notice that, for normal (vertical) incidence, the plane wave is TEM polarized, while here for the convenience of our description, the y-polarized wave is noted as TE incident and the x-polarized wave is noted as TM incident. As demonstrated in Fig. 5(a), when the proposed metasurface with a split θ is considered, in the initial scenario under TE incidence, the metasurface is of broken in-plane symmetry relative to IPD; when IPD is rotated, the net dipole moment contributed by the unequal dipole moment on each side of IPD will followingly decrease, causing the drop of the intensity of MD QBIC resonance and limiting its ability to boost the local field; and when under TM incidence, the metasurface becomes symmetrical again relative to IPD, which is equivalent to transform the QBIC mode back into another type of SPBIC supported by an alternative MD with equal dipole moment on each side of IPD (x axis). This equal MD will shut down the radiating channel, which makes the mode confined again and terminates the strong local-field enhancement.

Our further research has proved the mechanism above. Taking the proposed critical-coupling absorber with $\theta = 7.1^\circ$ and $E_F = 0.2$ eV, for example, we gradually rotate IPD with an angle α and test the absorption spectra, and the result is shown in Fig. 5(b). The result shows that the absorption peak decays with increasing α strictly at the same wavelength without shift. If separately considering the metasurface (without monolayer graphene), the transmission spectra also exhibit the similar shiftless behavior, as shown in Fig. 5(c). When it comes to the absorption spectra under TE incidence and TM incidence, as shown in Fig. 5(d), which lead to the highest and unenhanced absorption, respectively, the maximal difference of the absorbing intensity $\Delta\mathbf{A} \approx 0.485$, and the modulation efficiency reaches 97.1%. Such high efficiency exceeds many existing works [33,34]. We have also analyzed the decaying behavior of the absorption peak, and the result is shown in Fig. 5(e), where the peak absorbing intensity is plotted as a function of α and fitted in a Sine model:

$$\mathbf{A}_{peak}(\alpha) = 0.258 + 0.243 \sin\left[\frac{(\alpha + 43.973)\pi}{88.325}\right]. \tag{13}$$

All these signs indicate that the absorbing intensity of the graphene-metasurface system is related to the MD QBIC resonance. To prove this claim, MD intensity in the multipole responses of the metasurface under $\theta = 7.1^\circ$ is tested in Fig. 5(f). The result shows that from TE to TM incident, the MD response vanishes, correlating with Fig. 5(d). Moreover, with increasing α, the MD response also shows a gradual decrease, which is analyzed in Fig. 5(g), and fitted in a Sine model:

$$\mathrm{MD}_{peak}(\alpha) = 32220400 + 32221000 \sin\left[\frac{(\alpha + 44.994)\pi}{89.994}\right]. \tag{14}$$

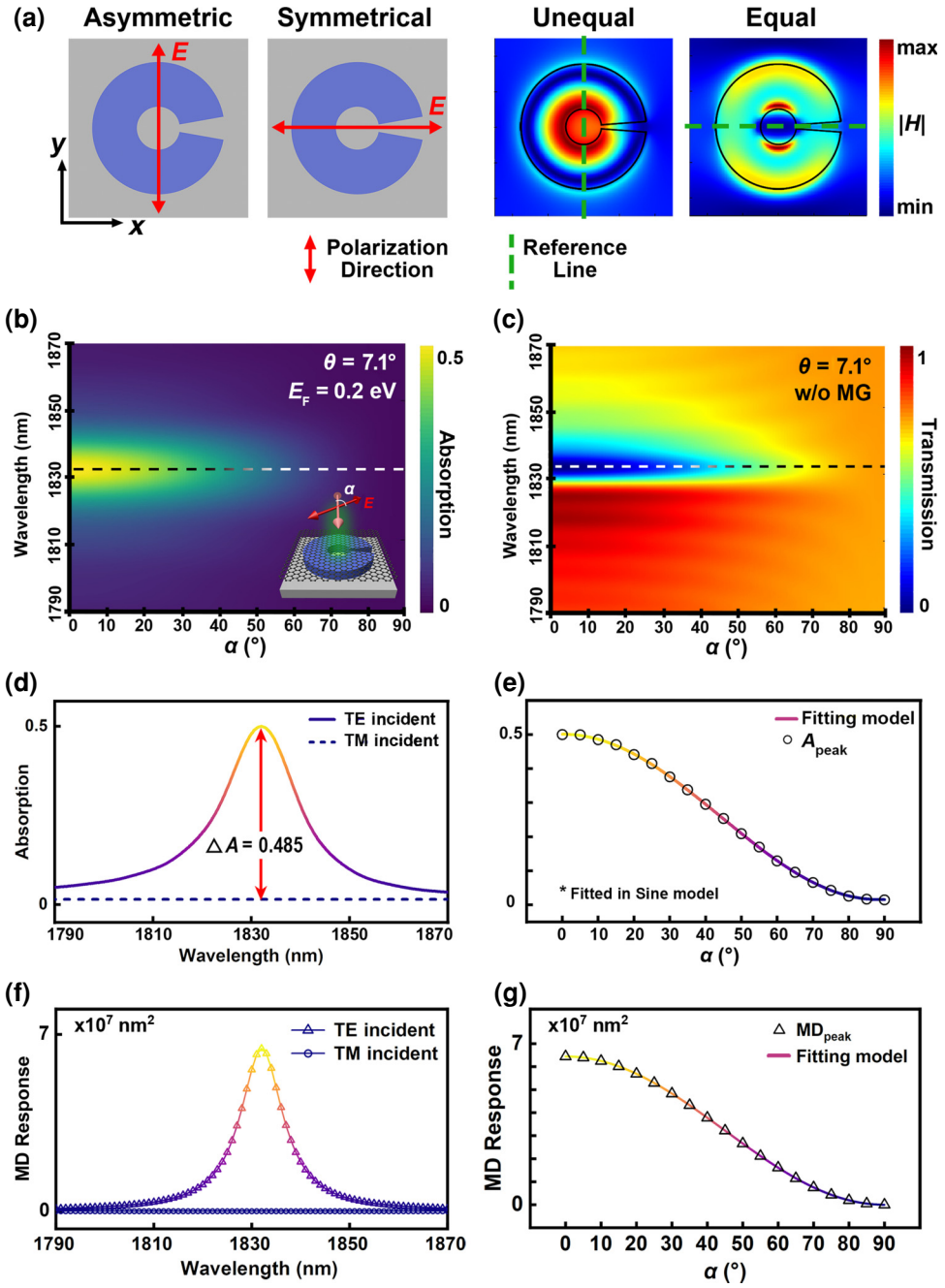

FIG. 5. (a) Examining the in-plane symmetry and excited MD with reference to IPD. (b) critical-coupling absorption spectra ($\theta = 7.1°$, $E_F = 0.2$ eV) under variant incident polarization α from 0° to 90°. The shiftless absorption peak is indicated by a dashed line. (c) Transmission spectra when $\theta = 7.1°$, under variant α from 0° to 90°. The shiftless transmission dip is indicated by a dashed line. (d) Absorption spectra of the critical coupling system under $\alpha = 0°$ and 90°, respectively. (e) The declined curve of the peak absorbing intensity in (b). (f) MD responses of the metasurface when $\theta = 7.1°$, under $\alpha = 0°$ and 90°, respectively. (g) The declined curve of the peak intensity of MD responses with variant α.

The Sine form of $\mathrm{MD}_{\mathrm{peak}}(\alpha)$ agrees well with $\mathbf{A}_{\mathrm{peak}}(\alpha)$, confirming that the polarization-sensitive MD resonance dominates the intensity of the maximized absorption.

Based on the above mechanism of polarization-modulating absorption in our proposed graphene-metasurface absorber, an optical digital "0-1" switching function is achieved. In the demonstration in Fig. 6(a), a 4×4 array is composed of the critical-coupling units with $\theta = 7.1°$ and $E_F = 0.2$ eV, for example, and exposed under the normal incident light. The amplitude of the transmitting light $|E|_{\mathrm{trans}}$ is used to measure the array's status. As shown in Fig. 6(b), when under the original incident plane wave

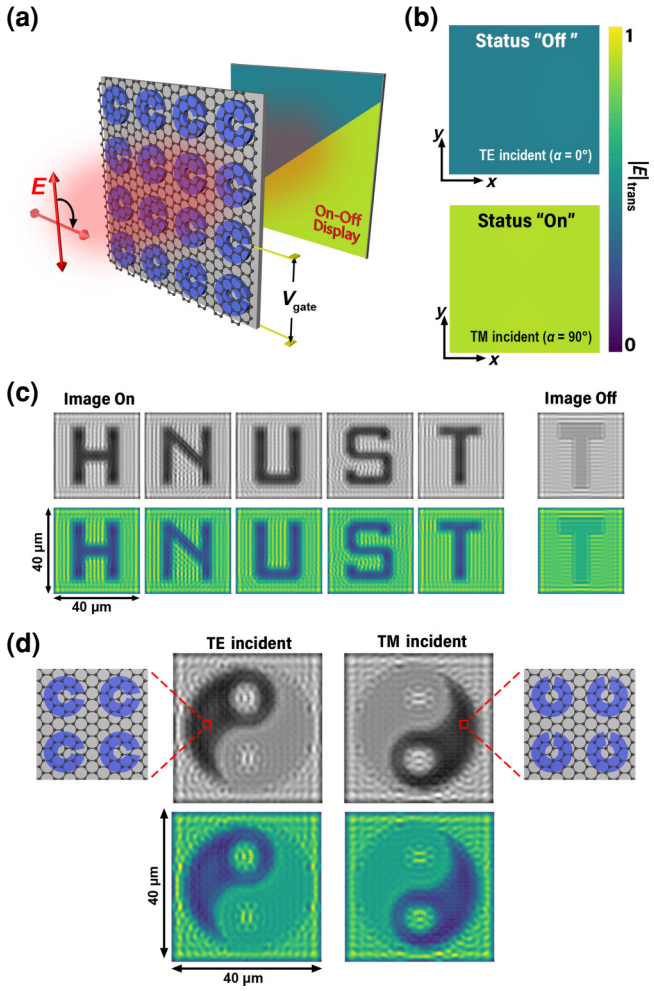

FIG. 6. (a) Schematic of the IPD-modulating "0-1" array, composed of the critical-coupling unit in Fig. 5(b). (b) Contrasted amplitude patterns of the transmitting light under TE and TM incidence, respectively, at $\lambda = 1831.99$ nm. (c) Demonstrations of the switchable image-displaying design for different letters in 40×40-pixel size, presented in grayscale and Viridis, which can be turned off by TM IPD. (d) Demonstrations of selecting the displaying part of the image by IPD in a "Tai Chi"-shaped array. The red boxes indicate differential designs for each part of the array.

(TE incident, $|E| = 1$) at the resonance frequency, QBIC is excited in the array, bringing maximized critical-coupling absorption, manifesting a dark $|E|_{\text{trans}}$ pattern, which can be defined as code "0" or status "off." When IPD is turned TM incident, the boosted absorption is terminated, which causes high transmission, manifesting a bright $|E|_{\text{trans}}$ pattern, which can be defined as code "1" or status "on." These two patterns with significant contrast are obtained in the same array, which means that the function can be realized by simply modulating IPD without any change in structure.

Moreover, based on the polarization-sensitive switching function, a switchable and selectable image-displaying function, which allows free design, is also achieved. Similarly, we use the proposed metasurface with $\theta = 7.1^\circ$ and $E_F = 0.2$ eV as a pixel ($1 \times 1\ \mu m^2$), and design images on a 40×40-pixel-sized SiO_2 substrate panel (and here for the sake of rigor, the periodic boundary conditions in x and y directions of the simulation region is modified to PMLs, to simulate the finite structural size in actual application). The results in Fig. 6(c), where we demonstrate the performance of displaying different letters at the critical-coupling wavelength $\lambda = 1831.99$ nm, present images of high and pronounced contrast, and such display can be switched off by manipulating IPD to TM incident. Furthermore, in Fig. 6(d), we demonstrate another function to select which part of the image array to display by IPD. The method is to arrange each part of the image with the original C-shaped rings and the rings rotated 90° anticlockwise, respectively, which is illustrated in the inset of Fig. 6(d). Therefore, due to the mechanism discussed in Fig. 5(a), under TE and TM incidence, respectively, QBIC will be separately excited in each differentially designed part of the image array to behave strong absorption and allow partial displaying selection. And from these results we deduce that, with enough computer resources to simulate larger arrays (i.e., more pixels), images with high-resolution ratio can be obtained. All the results presented above indicate promising potential applications in next-gen optical digital switches and image display devices.

Last but not least, it is worth mentioning that, research has proved that by increasing the uniaxial strain on graphene samples to flatten the corrugations and ripples, the random strain fluctuations (RSFs), the primary disorder causing electron scattering, can be efficiently reduced [54]. This method makes sense in maintaining a stable performance of the graphene samples in experiments. Moreover, in a recent study from Jin *et al.*, the authors successfully transferred the monolayer graphene onto the top plane of a metasurface in the experiment, and provided detailed fabrication methods [55]. Such exciting successes can provide solid technical support for the practical rationality of our study in possible further experiments. What is more, the topological insulators (TIs) with voltage-modulatable surface states, similar to the E_F of graphene, are regarded as promising materials for the next-gen optoelectronic devices. Recently, 2D germanene, the Ge analogue of graphene, has been successfully grown in experiments and proved to exhibit the TI natures [56]. This success may provide an exciting chance for the strong coupling between 2D TIs and QBIC metasurfaces. We hope the mechanisms we proposed in this paper can help pave the way for possible further studies on germanene-QBIC coupling systems and their applications.

IV. CONCLUSION

In summary, we have demonstrated a resonant germanium metasurface supporting MD-QBIC resonance. Due

to the strong local field enhancement originating from the QBIC nature, we have proved that such QBIC can significantly boost the light-graphene interaction, leading to enhanced graphene absorption. By optimizing the Fermi level of graphene and the asymmetry parameter of the metasurface, a tunable critical-coupling absorber was achieved. The influence of incident polarization was further considered. The results showed that the intensity of the enhanced absorption can be efficiently tuned by maneuvering the polarization direction, providing a high modulating efficiency up to 97.1%. Finally, we have also demonstrated the performance of "0-1" switching function and switchable and selectable image-displaying function through the polarization-controlling method. Our results may offer unique opportunities for constructing next-gen alternative photonic metadevices.

ACKNOWLEDMGENTS

The authors acknowledge the support provided by the National Natural Science Foundation of China (Grants No. 62275079 and No. 62175062), the Scientific Research Fund of Hunan Provincial Education Department (Grants No. 23A0454, No. 21B0581, and No. 21B0566), Changsha Municipal Natural Science Foundation (Grant No. kp2208059) and the Postgraduate Scientific Research Innovation Project of Hunan Province (Grant No. CX20231047).

[1] L. Novotny and B. Hecht in *Principles of Nano-Optics*, Vol. 90 (Cambridge University Press, Cambridge, 2006), p. 378.
[2] N. I. Zheludev and Y. S. Kivshar, From metamaterials to metadevices, Nat. Mater. **11**, 917 (2012).
[3] H. Chen, R. Kersting, and G. Cho, Terahertz imaging with nano-meter resolution, Appl. Phys. Lett. **83**, 3009 (2003).
[4] S. Pereira and S. LaRochelle, Field profiles and spectral properties of chirped Bragg grating Fabry-Perot interferometers, Opt. Express **13**, 1906 (2005).
[5] H. Song and T. Nagatsuma, Present and future of terahertz communications, IEEE Trans. Terahertz Sci. Technol. **1**, 256 (2011).
[6] A. Berkhout and A. F. Koenderink, Perfect absorption and phase singularities in plasmon antenna array etalons, ACS Photonics **6**, 2917 (2019).
[7] A. I. Kuznetsov, A. E. Miroshnichenko, M. L. Brongersma, Y. S. Kivshar, and B. Luk'yanchuk, Optically resonant dielectric nanostructures, Science **354**, aag2472 (2016).
[8] L. Huang, L. Xu, D. A. Powell, W. J. Padilla, and A. E. Miroshnichenko, Resonant leaky modes in all-dielectric metasystems: Fundamentals and applications, Phys. Rep. **1008**, 1 (2023).
[9] A. Krasnok, M. Tymchenko, and A. Alù, Nonlinear metasurfaces: A paradigm shift in nonlinear optics, Mater. Today **21**, 8 (2018).
[10] Z. Liu, G. Liu, X. Liu, J. Chen, and C. Tang, Spatial and frequency-selective optical field coupling absorption in an ultra-thin random metasurface, Opt. Lett. **48**, 1586 (2023).
[11] M. Tseng, Y. Jahani, A. Leitis, and H. Altug, Dielectric metasurfaces enabling advanced optical biosensors, ACS Photonics **8**, 47 (2021).
[12] A. Komar, R. A. Aoni, Lei Xu, M. Rahmani, A. E. Miroshnichenko, and D. N. Neshev, Edge detection with Mie-resonant dielectric metasurfaces, ACS Photonics **8**, 864 (2021).
[13] T. Kang, B. Fan, J. Qin, W. Yang, S. Xia, Z. Peng, B. Liu, S. Peng, X. Liang, T. Tang, L. Deng, Y. Luo, H. Wang, Q. Zhou, and L. Bi, Mid-infrared active metasurface based on Si/VO_2 hybrid meta-atoms, Photonics Res. **10**, 373 (2022).
[14] R. R. Nair, P. Blake, A. N. Grigorenko, K. S. Novoselov, T. J. Booth, T. Stauber, N. M. R. Peres, and A. K. Geim, Fine structure constant defines visual transparency of graphene, Science **320**, 1308 (2008).
[15] P. Jordan, J. V. Neumann, and E. P. Wigner, in *The Collected Works of Eugene Paul Wigner: Part A: The Scientific Papers* (Springer, Berlin, Heidelberg, 1993), p. 298.
[16] C. M. Linton and P. McIver, Embedded trapped modes in water waves and acoustics, Wave Motion **45**, 16 (2007).
[17] A. G. Every and A. A. Maznev, Fano line shapes of leaky surface acoustic waves extending from supersonic surface wave points, Wave Motion **79**, 1 (2018).
[18] A. F. Sadreev, Interference traps waves in an open system: Bound states in the continuum, Rep. Prog. Phys. **84**, 055901 (2021).
[19] S. Weimann, Yi Xu, R. Keil, A. E. Miroshnichenko, A. Tünnermann, S. Nolte, A. A. Sukhorukov, A. Szameit, and Y. S. Kivshar, Compact surface Fano states embedded in the continuum of waveguide arrays, Phys. Rev. Lett. **111**, 240403 (2013).
[20] D. C. Marinica, A. G. Borisov, and S. V. Shabanov, Bound states in the continuum in photonics, Phys. Rev. Lett. **100**, 183902 (2008).
[21] E. N. Bulgakov and A. F. Sadreev, Bloch bound states in the radiation continuum in a periodic array of dielectric rods, Phys. Rev. A **90**, 053801 (2014).
[22] J. Li, J. Li, C. Zheng, Z. Yue, S. Wang, M. Li, H. Zhao, Y. Zhang, and J. Yao, Free switch between bound states in the continuum (BIC) and quasi-BIC supported by graphene-metal terahertz metasurfaces, Carbon **182**, 506 (2021).
[23] F. Monticone and A. Alù, Bound states within the radiation continuum in diffraction gratings and the role of leaky modes, New J. Phys. **19**, 093011 (2017).
[24] D. R. Abujetas, N. van Hoof, S. ter Huurne, J. G. Rivas, and J. A. Sánchez-Gil, Spectral and temporal evidence of robust photonic bound states in the continuum on terahertz metasurfaces, Optica **6**, 996 (2019).
[25] V. R. Tuz, V. V. Khardikov, A. S. Kupriianov, K. L. Domina, S. Xu, H. Wang, and H.-B. Sun, High-quality trapped modes in all-dielectric metamaterials, Opt. Express **26**, 2905 (2018).
[26] C. Zhou, L. Huang, R. Jin, L. Xu, G. Li, M. Rahmani, X. Chen, W. Lu, and A. E. Miroshnichenko, Bound states in the continuum in asymmetric dielectric metasurfaces, Laser & Photonics Rev. **17**, 2200564 (2023).

[27] I. A. M. Al-Ani, K. As'Ham, L. Huang, A. E. Miroshnichenko, and H. T. Hattori, Enhanced strong coupling of TMDC monolayers by bound state in the continuum, Laser & Photonics Rev. **15**, 2100240 (2021).
[28] Y. Chen, C. Zhao, Y. Zhang, and C. Qiu, Integrated molar chiral sensing based on high-Q metasurface, Nano Lett. **20**, 8696 (2020).
[29] Y. Wang, Y. Fan, X. Zhang, H. Tang, Q. Song, J. Han, and S. Xiao, Highly controllable etchless perovskite microlasers based on bound states in the continuum, ACS Nano. **15**, 7386 (2021).
[30] E. Gao, Z. Liu, H. Li, H. Xu, Z. Zhang, X. Luo, C. Xiong, C. Liu, B. Zhang, and F. Zhou, Dynamically tunable dual plasmon-induced transparency and absorption based on a single-layer patterned graphene metamaterial, Opt. Express **27**, 13884 (2019).
[31] K. Sun, H. Jiang, D. A. Bykov, V. Van, U. Levy, Y. Cai, and Z. Han, 1D quasi-bound states in the continuum with large operation bandwidth in the $\omega \sim k$ space for nonlinear optical applications, Photonics Res. **10**, 1575 (2022).
[32] R. Zhou, T. Guo, L. Huang, and K. Ullah, Engineering the harmonic generation in graphene, Mater. Today Phys. **23**, 100649 (2022).
[33] Z. Liu, X. Zhang, Z. Zhang, E. Gao, F. Zhou, H. Li, and X. Luo, Simultaneous switching at multiple frequencies and triple plasmon-induced transparency in multilayer patterned graphene-based terahertz metamaterial, New J. Phys. **22**, 083006 (2020).
[34] A. Mujahid, M. Imran, H. Fan, I. Ahmed, T. Yuan, Z. Feng, F. Nadeem, and Y. Zhang, Temporal and spectral hybrid bound state in continuum and its reliance on the correlation, Phys. Chem. Chem. Phys. **24**, 12457 (2022).
[35] X. Zhang, Z. Liu, Z. Zhang, E. Gao, X. Luo, F. Zhou, H. Li, and Z. Yi, Polarization-sensitive triple plasmon-induced transparency with synchronous and asynchronous switching based on monolayer graphene metamaterials, Opt. Express **28**, 36771 (2020).
[36] L. Xu, Khosro Zangeneh Kamali, L. Huang, M. Rahmani, A. Smirnov, R. Camacho-Morales, Y. Ma, G. Zhang, M. Woolley, D. Neshev, and A. E. Miroshnichenko, Dynamic nonlinear image tuning through magnetic dipole quasi-BIC ultrathin resonators, Adv. Sci. **6**, 1802119 (2019).
[37] T. Hinamoto and M. Fujii, MENP: An open-source MATLAB implementation of multipole expansion for nanophotonics, Osa Continuum **4**, 1640 (2021).
[38] K. Koshelev, S. Lepeshov, M. Liu, A. Bogdanov, and Y. Kivshar, Asymmetric metasurfaces with high-Q resonances governed by bound states in the continuum, Phys. Rev. Lett. **121**, 193903 (2018).
[39] X. Zhu, L. Shi, M. S. Schmidt, A. Boisen, O. Hansen, J. Zi, S. Xiao, and N. A. Mortensen, Enhanced light–matter interactions in graphene-covered gold nanovoid arrays, Nano Lett. **13**, 4690 (2013).
[40] K. Ziegler, Minimal conductivity of graphene: Nonuniversal values from the Kubo formula, Phys. Rev. B **75**, 233407 (2007).
[41] Q. Li, L. Cong, R. Singh, N. Xu, W. Cao, X. Zhang, Z. Tian, L. Du, J. Han, and W. Zhang, Monolayer graphene sensing enabled by the strong Fano-resonant metasurface, Nanoscale **8**, 17278 (2016).
[42] S. Fan, W. Suh, and J. D. Joannopoulos, Temporal coupled-mode theory for the Fano resonance in optical resonators, J. Opt. Soc. Am. A **20**, 569 (2003).
[43] H. A. Haus, *Waves and Fields in Optoelectronics* (Prentice Hall, Upper Saddle River, New Jersey, 1984), Chap. 7.
[44] R. Masoudian, L. Huang, and A. Miroshnichenko, Polarization-independent perfect absorber enabled by quasi-bound states in the continuum, Phys. Rev. B **104**, 235405 (2021).
[45] B. Song, H. Gu, S. Zhu, H. Jiang, X. Chen, C. Zhang, and S. Liu, Broadband optical properties of graphene and HOPG investigated by spectroscopic mueller matrix ellipsometry, Appl. Surf. Sci. **439**, 1079 (2018).
[46] A. Vakil and N. Engheta, Transformation optics using graphene, Science **332**, 1291 (2011).
[47] S. Xiao, T. Liu, X. Wang, X. Liu, and C. Zhou, Tailoring the absorption bandwidth of graphene at critical coupling, Phys. Rev. B **102**, 085410 (2020).
[48] X. Wang, J. Duan, W. Chen, C. Zhou, T. Liu, and S. Xiao, Controlling light absorption of graphene at critical coupling through magnetic dipole quasi-bound states in the continuum resonance, Phys. Rev. B **102**, 155432 (2020).
[49] Y. Cai, Y. Huang, K. Zhu, and H. Wu, Symmetric metasurface with dual band polarization-independent high-Q resonances governed by symmetry-protected BIC, Opt. Lett. **46**, 4049 (2021).
[50] C. Liu, H. Li, H. Xu, M. Zhao, C. Xiong, M. Li, B. Ruan, B. Zhang, and K. Wu, Plasmonic biosensor based on excellently absorbable adjustable plasmon-induced transparency in black phosphorus and graphene metamaterials, New J. Phys. **22**, 073049 (2020).
[51] T. Chen, W. Jiang, and X. Yin, Dual-band ultrasensitive terahertz sensor based on tunable graphene metamaterial absorber, Superlattice Microst. **154**, 106898 (2021).
[52] K. Fan, J. Y. Suen, X. Liu, and W. J. Padilla, All-dielectric metasurface absorbers for uncooled terahertz imaging, Optica **4**, 601 (2017).
[53] Q. Yang, M. Liu, S. Kruk, Y. Xu, Y. K. Srivastava, R. Singh, J. Han, Y. Kivshar, and I. V. Shadrivov, Polarization-sensitive dielectric membrane metasurfaces, Adv. Opt. Mater. **8**, 2000555 (2020).
[54] L. Wang, P. Makk, S. Zihlmann, A. Baumgartner, D. I. Indolese, K. Watanabe, T. Taniguchi, and C. Schönenberger, Mobility enhancement in graphene by in situ reduction of random strain fluctuations, Phys. Rev. Lett. **124**, 157701 (2020).
[55] R. Jin, L. Huang, C. Zhou, J. Guo, Z. Fu, J. Chen, J. Wang, X. Li, F. Yu, J. Chen, Z. Zhao, X. Chen, W. Lu, and G. Li, Toroidal dipole BIC-driven highly robust perfect absorption with a graphene-loaded metasurface, Nano Lett. **23**, 9105 (2023).
[56] P. Bampoulis, C. Castenmiller, D. Klaassen, J. van Mil, Y. Liu, C. C. Liu, Y. Yao, M. Ezawa, A. Rudenko, and H. Zandvliet, Quantum spin Hall states and topological phase transition in germanene, Phys. Rev. Lett. **130**, 196401 (2023).